



Deep and near-surface consequences of root removal by asymmetric continental delamination

J.L. Valera^{a,*}, A.M. Negrodo^a, I. Jiménez-Munt^b

^a Dept. of Geophysics, Faculty of Physics, Universidad Complutense de Madrid, Av. Complutense s/n.28040 Madrid, Spain

^b Instituto de Ciencias de la Tierra 'Jaume Almera', CSIC, C/Sole i Sabaris s/n. 08028 Barcelona, Spain

ARTICLE INFO

Article history:

Received 31 July 2009

Received in revised form 3 March 2010

Accepted 1 April 2010

Available online 10 April 2010

Keywords:

Continental delamination

Topography evolution

Thermo-mechanical modeling

Numerical algorithm

ABSTRACT

The occurrence of continental delamination has been proposed for a number of areas characterized by highly variable geodynamic settings. In this study we present results of numerical simulations considering different initial setups, representative for geodynamic scenarios where delamination could potentially develop. To mimic a post-collisional orogenic scenario we have designed an initial state characterized by the presence of an area of orogenic lithosphere, with both crustal and lithospheric roots. In a second setup, we have considered a lithospheric root representative of a remnant slab with a flat overlying crust. We focus on predicted evolution of surface and near-surface observables, namely the crustal structure, surface heat flow and isostatic and dynamic topography evolution. Our results show that a high density orogenic lower crust, likely related to the presence of eclogite, significantly accelerates the sinking of the lithospheric mantle. The pattern of local isostatic elevation is characterized by laterally migrating surface uplift/subsidence. This pattern is shown to be little sensitive to lower crust density variations. In contrast, predicted dynamic topography is more sensitive to these changes, and shows surface subsidence adjacent to the delaminating lithospheric mantle for the model with a high density lower crust, and surface uplift above the slab for a model with a less dense lower crust. The reason for uplift in this second model is that the effect of the positive buoyancy of the thickened crust overwhelms the effect of negative buoyancy of the slowly sinking lithospheric mantle. We infer from our modeling that there is not a specific characteristic pattern of topography changes associated with delamination, but it depends on the interplay between highly variable factors, as slab sinking velocity, asthenospheric upwelling and changes in crustal thickness.

© 2010 Elsevier B.V. All rights reserved.

1. Introduction

Removal of continental lithospheric mantle has been inferred from a wide range of observations. The most significant includes anomalously high heat flow, regional uplift, change of stress field toward extension, and the presence of cold slabs in the upper mantle and igneous activity in continental areas far from present subduction zones. The processes responsible for removal of continental lithospheric mantle are still under debate, but most of the related models presented during the last 30 years can be grouped into two categories: those based on viscous convective removal and those based on lithospheric delamination.

The convective removal mechanism is based on the fact that a thickened thermal boundary layer (mantle lithosphere) can develop a Rayleigh–Taylor gravitational instability and drip viscously into the less dense asthenosphere. This mechanism has been extensively investigated in a series of studies using dynamic approaches (e.g.

Houseman et al., 1981; England and Houseman, 1989; see Houseman and Molnar, 2001 for a thorough revision) and in a number of studies adopting thermo-mechanical approaches (e.g. Fleitout and Froidevaux, 1982; Buck and Toksöz, 1983; Lenardic and Kaula, 1995; Marotta et al., 1998; Schott and Schmeling, 1998).

The continental delamination mechanism was introduced by Bird (1978, 1979), who proposed that if any process provided an elongated conduit connecting the underlying asthenosphere with the base of the continental crust, the dense lithospheric boundary layer could peel away from the crust and sink. Differently from convective removal, where the lithospheric root deforms internally as it drips, in the case of delamination the mantle part of the lithosphere peels away as a coherent slice, without necessarily undergoing major internal deformation, and is replaced by buoyant asthenosphere. To avoid ambiguity commonly found in the literature, where the term 'delamination' is often used to refer to any process causing removal of lithosphere, it is worth clarifying that in this study we will only use the term 'delamination' when two conditions of Bird's model are fulfilled: 1) the asthenosphere comes into direct contact with the crust and 2) the point of delamination, where the lithosphere peels off the overlying crust, migrates.

* Corresponding author.

E-mail addresses: jvalera@fis.ucm.es (J.L. Valera), anegredo@fis.ucm.es (A.M. Negrodo), ivone@ictja.csic.es (I. Jiménez-Munt).

Delamination has been proposed for a number of geological areas. Some examples are Tibet and Colorado plateaus (Bird, 1978 and 1979, respectively), western Mediterranean (Channel and Mareschal, 1989), Variscan belt (Arnold et al., 2001), Alboran sea (e.g. Seber et al., 1996; Calvert et al., 2000; Valera et al., 2008); Sierra Nevada mountains (Ducea and Saleeby, 1998; Zandt et al., 2004; Le Pourhiet et al., 2006), Vrancea region (Knapp et al., 2005) and eastern Anatolia (Göğüş and Pysklywec, 2008a). In spite of this large number of examples, the very few physical models that have been developed (e.g. Schott and Schmeling, 1998; Morency and Doin, 2004); make that basic aspects of the delamination process remain poorly studied.

Very recently, Göğüş and Pysklywec (2008b) presented a comparison between near-surface observables resulting from a model representative of delamination, and from two models of viscous dripping representative of partial and full mantle lithosphere removal. Differences in surface topography and P - T - t paths predicted by Göğüş and Pysklywec (2008b) with delamination and convective removal models reflect major differences in the style of crustal deformation and mantle lithosphere evolution resulting from both processes. These differences were also investigated in the study by Valera et al. (2008), who evaluated quantitatively conceptual models of delamination and convective removal proposed for the evolution of the Alboran Sea and surrounding regions.

In this study we present results of numerical simulations considering different initial setups, representative for different geodynamic scenarios likely prone to develop delamination. We focus on predicted evolution of surface and near-surface observables, namely the crustal structure, topographic response (both isostatic and dynamic) and surface heat flow.

It is worth noting that in some areas (e.g. Alboran sea and Pannonian basin) there is a strong controversial between authors proposing propagating continental delamination and those proposing migration of subduction caused by slab roll-back. In this sense, exploring the consequences of delamination on lithospheric and near-surface scales can also be helpful to discriminate between slab 'roll-back' and mantle lithosphere 'peel-back'.

2. Model description

2.1. Governing equations

The physical process of delamination is governed by the coupled conservation equations of mass, momentum and energy. We have applied several hypotheses to simplify these equations. First, we have assumed two-dimensional flow. Second, we have neglected inertial forces. This hypothesis can only be applied to very viscous flows, so with very high Prandtl number fluids. Third, we have applied the Extended Boussinesq Approximation (EBA). According to the Standard Boussinesq Approximation (Boussinesq, 1903), density variations may be neglected except when they are coupled to the gravitational acceleration in the buoyancy force term. The EBA differs from the Standard Boussinesq Approximation in that the thermal effect of compression is also accounted for (e.g., Tritton, 1988; Schmeling, 1989; Ita and King, 1994). Neglecting the inertial forces in a viscous flow under the EBA implies that the fluid is incompressible, which simplifies the equation of mass conservation.

The final equations are the same as those used by Valera et al. (2008), but we have neglected the shear heating and the effect of the phase transformation from olivine to high-pressure polymorphs. The reader is referred to Valera et al. (2008) for detailed explanations on the mathematical developments leading to equations:

$$\frac{\partial}{\partial x} \rho g = 4 \frac{\partial^2}{\partial x \partial z} \left[u \frac{\partial^2}{\partial x \partial z} \Psi \right] + \left(\frac{\partial^2}{\partial z^2} - \frac{\partial^2}{\partial x^2} \right) \left[u \left(\frac{\partial^2}{\partial z^2} - \frac{\partial^2}{\partial x^2} \right) \Psi \right] \quad (1)$$

$$\frac{\partial T}{\partial t} + u_x \frac{\partial T}{\partial x} + u_z \frac{\partial T}{\partial z} = \frac{H}{C_p} + \frac{k}{\rho C_p} \left(\frac{\partial^2 T}{\partial x^2} + \frac{\partial^2 T}{\partial z^2} \right) + u_z \frac{\alpha g}{C_p} T \quad (2)$$

where u_k is the k -component of the velocity vector; x is the horizontal coordinate; z is the vertical coordinate, pointing downward; μ is the viscosity; ρ is the density; g is the acceleration of gravity; C_p , the specific heat; T , the temperature; t is the time; H , the radiogenic heat production; k , the thermal conductivity; and α , the thermal expansion coefficient. The velocity is related to the stream function Ψ as:

$$u_x = \frac{\partial \Psi}{\partial z}; \quad u_z = -\frac{\partial \Psi}{\partial x}. \quad (3)$$

The heat sources considered here are the terms on the right-hand side of Eq. (2) and correspond to: the radiogenic heat production, the heat conduction and the adiabatic heating. The values of the parameters used are listed in Table 1.

Our modeled domain includes five different materials: upper crust, non-perturbed lower crust, orogenic lower crust, lithospheric mantle and asthenosphere (with asthenosphere we refer to the whole sub-lithospheric upper mantle). In some models we have introduced a sixth material on the top of the model, that will be described later on. For simplicity, density and viscosity have constant values in the upper and lower crust (see Table 1). The boundary between the lithospheric mantle and the asthenosphere is assumed to be a thermal boundary, with no compositional difference. Density and viscosity are assumed to be temperature dependent in the lithospheric mantle and asthenosphere. We have used a Newtonian temperature-dependent (exponential) viscosity law and augmented it with a pressure dependence that crudely simulates an increase in 'deeper mantle' viscosity beneath 450 km (Rüpke et al., 2004):

$$\mu(T, z) = \mu_0 \mu(z) \exp \left[b \left(\frac{T_0}{T} - 1 \right) \right] \quad (4)$$

Table 1

Parameters used in all calculations.

Symbol	Meaning	Value
g	Acceleration of gravity	9.8 ms ⁻²
Q_b	Basal heat flow	0.014 W m ⁻²
b	b -parameter of Rüpke Law	15
H_p	Crustal radiogenic heat production	8 × 10 ⁻⁷ W m ⁻³
	Horizontal extent	1376 km
	Vertical extent	680 km
C_p	Specific heat	1.3 × 10 ³ J K ⁻¹ kg ⁻¹
T_0	Temperature at the base of the lithosphere	1350 °C
k	Thermal conductivity	3.2 W m ⁻¹ K ⁻¹
α	Thermal expansion coefficient	3.7 × 10 ⁻⁵ K ⁻¹
	Time step	0.25 Ma
L	Lithospheric thickness	120 km
	Lower bound for the viscosity	10 ¹⁷ Pa s
	Upper bound for the viscosity	10 ²² Pa s
w_{\max_L}	Maximum amplitude of the Lithospheric Mantle perturbation	121.8 km
w_{\max_LC}	Maximum amplitude of the Lower Crust perturbation	33 km
w_{\max_UC}	Maximum amplitude of the Upper Crust perturbation	15 km
λ	Wavelength of the perturbation	487.2 km
x_{pert}	Horizontal position of the center of the perturbation	688 km
h_{UC}	Upper Crust thickness	15 km
ρ_{UC}	Upper Crust density	2800 kg m ⁻³
μ_{UC}	Upper Crust viscosity	10 ²⁰ Pa s
h_{LC}	Lower Crust thickness	22 km
ρ_{npLC}	Lower Crust density (non-perturbed zone)	2900 kg m ⁻³
μ_{npLC}	Lower Crust viscosity (non-perturbed zone)	10 ²⁰ Pa s
ρ_{LC}	Orogenic Lower Crust density (perturbed zone)	Variable
μ_{LC}	Orogenic Lower Crust viscosity (perturbed zone)	10 ²⁰ Pa s

$$\mu(z) = 1 + 124.5\{1 + \tanh[0.01(z-450)]\} \quad (5)$$

where μ_0 is a reference viscosity for each material; b is a parameter characterizing the temperature dependence of viscosity; and T_0 is the reference temperature at the base of the lithospheric mantle. The values of all these parameters are given in Table 1.

For the sake of simplicity and because of computational advantages, a linear rheology is assumed in our numerical modeling, as in many models (e.g. Enns et al., 2005; Marotta et al., 2006; Conrad et al., 2007; Manea and Gurnis, 2007). The use of non-linear rheology in models with a high number of different materials would require consideration of an extraordinary high number of poorly constrained rheological parameters. To promote coherent behavior of the lithospheric mantle (instead of dripping at its base), an upper bound (μ_{\max}) has been imposed to the mantle viscosity. This maximum value is reached at low temperatures, meaning shallow depths, in the lithospheric mantle. Due to the oversimplification of using a linear rheology, the computed viscosity values should be considered as an effective or equivalent viscosity.

2.2. Numerical approach

We have applied a second order, central finite difference scheme to discretize the motion equation. To solve the thermal equation we have applied a second order, central ADI (Alternative Difference Implicit) scheme combined with the Thomas Algorithm. The reader is referred to Negredo et al. (2004) for details on numerical solution of the thermal equation and to Valera et al. (2008) for a detailed explanation on the coupled solution of motion and thermal equation. We have used the thermo-mechanical numerical algorithm TEMESCH developed by Valera et al. (2008) in MATLAB code. We have considered free slip boundary conditions at all boundaries. The surface temperature is fixed at 0 °C, a constant heat flow computed from the initial geotherm is forced at the bottom and zero horizontal heat flow at the side boundaries (Fig. 1a).

We have used two different grids: an Eulerian grid with fixed nodes and a Lagrangian grid with moving markers carrying the material properties. The Eulerian grid is a Cartesian box of aspect ratio 2 with a resolution of 173×86 nodes in the x - and z -directions and a step-size of 8 km. The Lagrangian grid has three times more markers than nodes in each direction. The horizontal extent of the box is chosen large enough to prevent boundary effects. The convergence of

the results has been checked varying the spatial and time resolution and controlling the Courant criterion (e.g. Anderson, 1995).

2.3. Initial configurations

To study the role of initial crustal structure on the asymmetric delamination mechanism, we have performed two sets of models representative of different scenarios: a post-collisional orogenic scenario and a post slab break-off scenario.

To mimic a post-collisional orogenic scenario we have assumed an initial state characterized by the presence of an area of orogenic lithosphere, with both crustal and lithospheric roots. This same initial geometry was used by Valera et al. (2008) to evaluate the conceptual model of delamination proposed by Calvert et al. (2000) for the Alboran Sea. Following Schott and Schmeling (1998), we have adopted a sinus shape for the orogenic root. The wave amplitude w of the perturbation is computed with this expression:

$$w = h + w_{\max} \cos\left(\frac{2\pi(x-x_{\text{pert}})}{\lambda}\right) \quad (6)$$

where h is the non-perturbed thickness of the layer; w_{\max} is the maximum perturbation amplitude; x is the horizontal coordinate; x_{pert} is the position of the perturbation (at the center of the box); and λ is the wavelength of the perturbation (see Table 1). The base of the upper, lower crust and lithospheric mantle is modified according to this equation to mimic a lithospheric root. The perturbed thickness of each layer doubles its non-perturbed thickness.

The initial geotherm for the crust and lithospheric mantle is given by the steady-state solution of the heat conduction equation, whereas an adiabatic initial temperature profile is assumed for the asthenosphere (Negredo et al., 2004). In the orogenic zone, the isotherms are displaced downwards following the shape of the crustal and lithospheric roots.

For this setup we obtain a set of simulations by varying the density of the lower crust in the perturbed (orogenic) zone. High values of orogenic lower crust density in some simulations are intended to explore the effect of the presence of eclogite (e.g. Leech, 2001; Jull and Kelemen, 2001; Lustrino, 2005), and are consistent with previous numerical modeling of orogens (e.g., Schott and Schmeling, 1998; Jiménez-Munt et al., 2008). Mean viscosity values for the lithospheric mantle are in the range of those used by previous studies (e.g. Schott

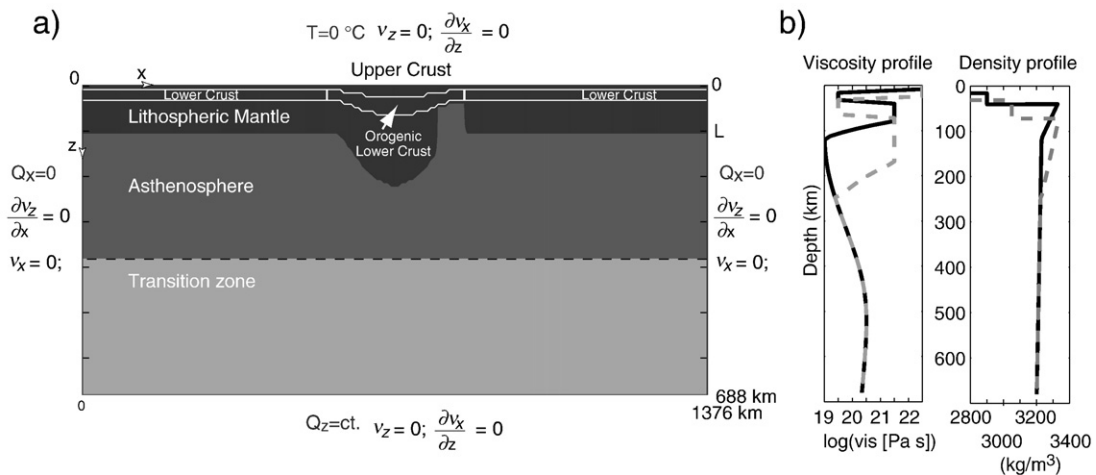


Fig. 1. a) Model domain illustrating the initial geometry and boundary conditions. b) Viscosity and density profiles used for the Reference Model at the initial state for an unperturbed column (solid lines) and for a column located at the center of the perturbation (dashed lines).

and Schmeling, 1998; Marotta et al., 1999; Morency and Doin, 2004; Gerya et al., 2004; Marotta et al., 2006; Göğüş and Pysklywec, 2008b). Fig. 1b shows the viscosity and density profiles used for the Reference Model of this setup at the initial state.

Adjacent to the lithospheric root, we have imposed a narrow ‘low viscosity conduit’ connecting the lower crust with the asthenosphere. Different mechanisms have been proposed to enable the ascent of asthenospheric material to the base of the crust. Bird (1979) argued that long cracks in lithosphere occur occasionally when continents break up around a new spreading center. This author also suggests that a hot rising ‘plume’ under a relatively moving plate might erode a continental plate up to the Moho. Turcotte (1983) proposed that asthenosphere can rise through a volcanic line associated with a subduction zone. Schott and Schmeling (1998) introduced a wide low viscosity zone, of about 200 km width, to enhance the input of asthenospheric material into the Moho and proposed this ‘low viscosity zone’ as a relict of a previous subduction, in which the dehydration reactions in the slab minerals released water creating a hydrated low viscosity zone above the slab. Arcay et al. (2007) performed 2D numerical thermo-mechanical modeling of subduction including the mantle wedge flow and the weakening effect in the mantle rocks due to the presence of water. Their results show that this weakening can produce a strong thermal thinning in the upper plate above the hydrated zone. Following this idea of thermal thinning, we have assumed that the conduit is filled with asthenospheric material, with the same composition but hotter than surrounding lithospheric mantle.

To model the evolution of dynamic topography we have performed another set of simulations for the same scenario (it means, same crustal structure), in which, following previous works (e.g. Gerya et al., 2004; Schmeling et al., 2008), a highly buoyant upper layer of very low viscosity has been included. This layer, whose initial thickness is 8 km, can be interpreted as a “sticky air” or an artificial layer whose lowermost part consists of water-rich, weak sediments, in short “soft sediments”. The interface between this layer and the top

of the crust is then treated as a free surface. We track motion of markers at this ‘free surface’ to compute changes in topography. We will refer to this computed topography as ‘dynamic topography’.

For the second model setup, we assume a flat geometry for the crust, and a mantle lithospheric root reaching the same depth as in the first setup. This configuration is intended to mimic a scenario where thickened lithospheric mantle represents the remnant of subduction after slab break-off. As for the first setup, we perform a set of simulations introducing the ‘soft sediments’ layer that allows for modeling topographic changes.

3. Model results

3.1. Models with crustal and lithospheric roots

The evolution of our Reference Model (Fig. 2), with an orogenic lower crust of 3050 kg m^{-3} , is similar to the evolution presented for the Alboran Sea by Valera et al. (2008) but much faster. The delamination mechanism initiates as the asthenospheric material rises through the conduit and widens it, pushing the orogenic thickened lithosphere to the left. This leftwards migration of the delamination tugs at the thickened crust and produces crustal/lithospheric thickening in front of the migrating delamination point and crustal/lithospheric thinning behind it. The room vacated by the migrating lithospheric mantle is filled up by the ascent of asthenospheric mantle up to the Moho. This coupled crustal thickening/thinning can also be observed in the models by Schott and Schmeling (1998) and by Göğüş and Pysklywec (2008b). Therefore, this coupled pattern can be considered as a characteristic feature of the delamination mechanism.

After only 5 Ma, the asthenospheric material begins to peel away the lithospheric mantle off the crust and sinks into the asthenosphere. The crustal thickening placed over the hinge of the sinking lithospheric mantle is displaced leftwards accompanying the lateral migration of the delamination point. Lower crustal material is pulled

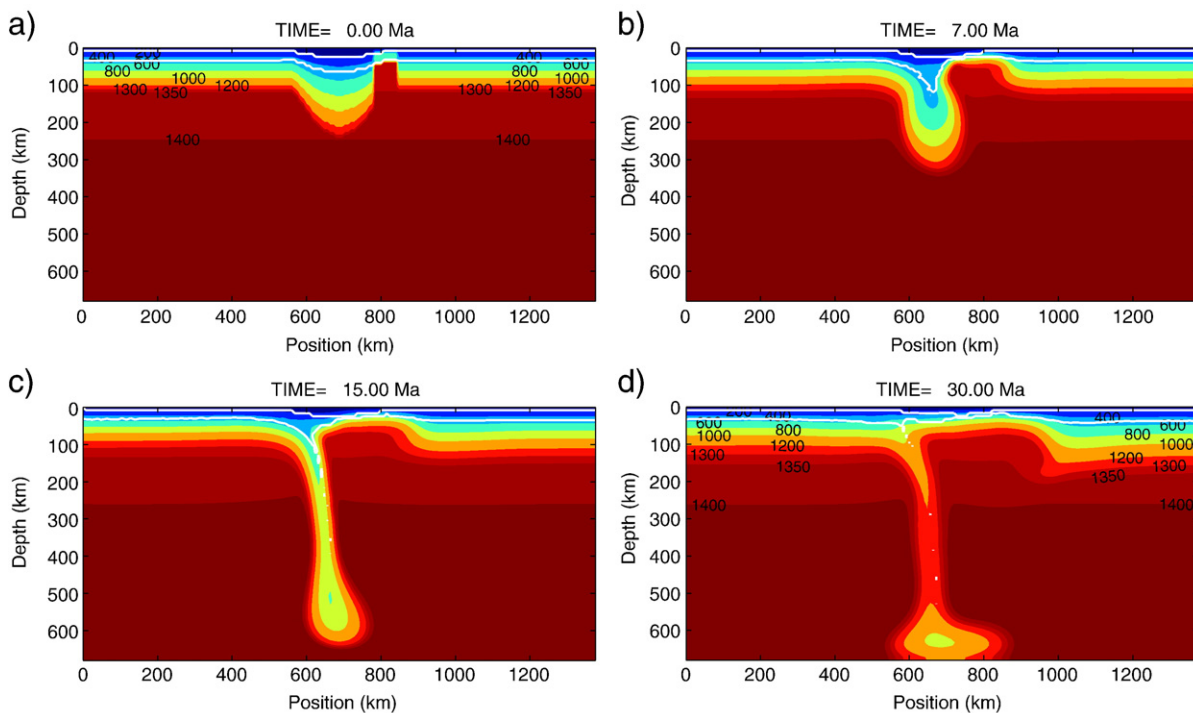


Fig. 2. Evolution of the Reference Model for the delamination process. Colors represent temperature distribution with labels in °C; white lines show the bases of the upper and lower crust.

down by viscous drag, and the Moho reaches depths of about 100–130 km around 15 Ma. The shape adopted by the dragged crust is a thin vertically elongated layer over the sinking lithospheric material, which is similar to the typical shape adopted by crust in an oceanic subduction zone. A similar Moho geometry was found by Schott and Schmeling (1998) who also predicted that significant amounts of lower crustal material were subducted into the mantle during delamination. On the other hand, the crustal thinning behind the migrating point achieves, after about 7 Ma, a maximum thinning factor (initial Moho depth divided by its current depth) of 2.7.

After about 12 Ma the delaminated slab of lithospheric mantle reaches a depth of about 600 km and begins to interact with the more viscous deepest part of the upper mantle. Therefore, the delaminated slab bends and lays over the lower boundary (the upper–lower mantle boundary), and the neck of the slab starts thinning due to conductive heating from the surrounding mantle. The viscous drag force decreases, so the buoyant lower crust ascends to achieve the dynamic equilibrium. This process also produces little migration of the delamination point.

We have performed additional tests (not shown) that indicate that the results are qualitatively the same if the ‘asthenospheric conduit’ was filled with low viscosity lithospheric material.

The set of parameters in this Reference Model has been chosen on the basis of reproducing a fast and well developed delamination process. For this purpose, we have performed a set of different models with the same crustal structure but varying the maximum viscosity of the lithospheric mantle (μ_{max}), the viscosity of the orogenic lower crust (μ_{LC}) and the reference viscosity of the asthenosphere (μ_0). Fig. 3 shows the accumulated displacement of the delamination point at 30 Ma for this set of models. According to these results, reducing the values of any of these viscosities favors delamination and increasing any of these values hinders the delamination process (Valera, 2009). On the basis of this parametric analysis, a low value of the maximum lithospheric viscosity was adopted for our Reference Model. Such low value enhances the coherent behavior of the lithospheric mantle, producing a mobile lithospheric mantle which is easily separated from the crust by the horizontal intrusion of the asthenospheric material.

We also show for the Reference Model the evolution of surface heat flow and of local isostatic topography (Fig. 4). Evolution of model-predicted heat flow reflects both thermal relaxation from the initial strongly heterogeneous thermal state, and widening of the area of asthenospheric upwelling. Elevation is calculated for every column of the mesh by comparing its buoyancy with that corresponding to the

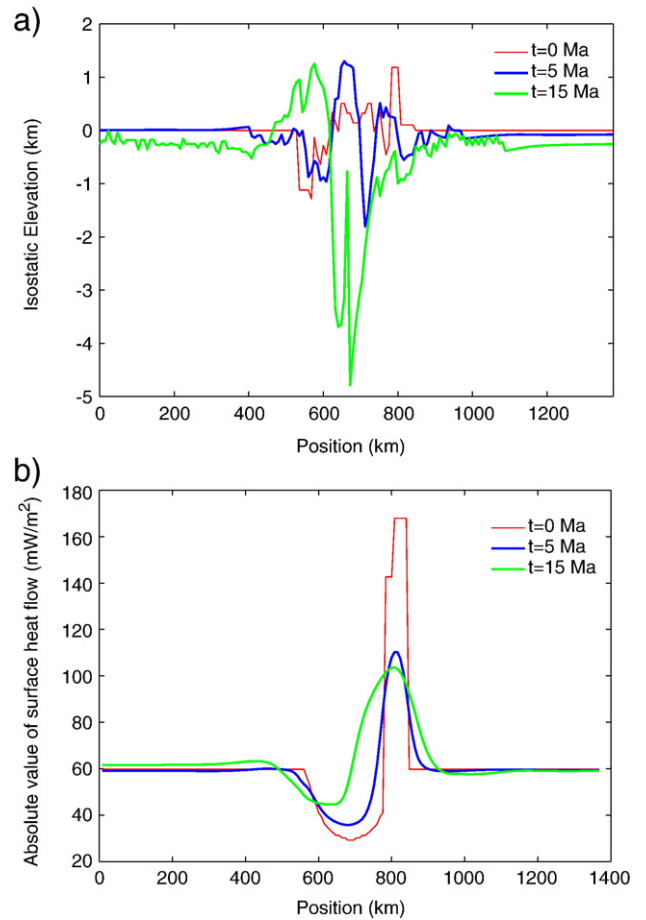


Fig. 4. Evolution of local isostatic topography (a) and of surface heat flow (b) for the Reference Model.

column at the left boundary of the model under the assumption of local isostasy and following Lachenbruch and Morgan (1990). The depth of isostatic compensation is taken at the maximum depth of the model. We are aware that the local isostasy hypothesis is not appropriate for delamination due to the presence of a dipping slab and to significant material motion. However, we have applied, at a first stage, the local isostasy hypothesis to obtain a first order estimation of the uplift/subsidence pattern as a consequence of the mass redistribution. Moreover, comparison with model-predicted dynamic topography will permit us to evaluate how much of the topographic response is captured by local isostatic topography. The model-predicted evolution of local isostatic topography shows a leftwards migrating pattern of uplift/subsidence, following the leftwards migration of delaminating lithospheric mantle and of crustal thickening over the slab.

Fig. 5 shows a comparison after 15 Ma of evolution of the Reference Model and another one with a less dense lower crust. It is remarkable that by reducing only the density of the orogenic lower crust the delamination process is significantly decelerated. We can therefore infer that, at least for this orogenic crust initial configuration, the density of the orogenic lower crust strongly affects the development of delamination. However, the pattern of predicted surface heat flow is rather similar for both models. In this figure, comparison with density distribution facilitates the interpretation of the predicted pattern of uplift/subsidence. In the Reference Model, predicted uplift between about 450 and 620 km is the response to crustal thickening. Further to the right, until about 750 km, strong subsidence is the response to the density excess related to the presence of the slab. Between about 750 and 900 km, the mass deficit related to mantle lithospheric thinning is

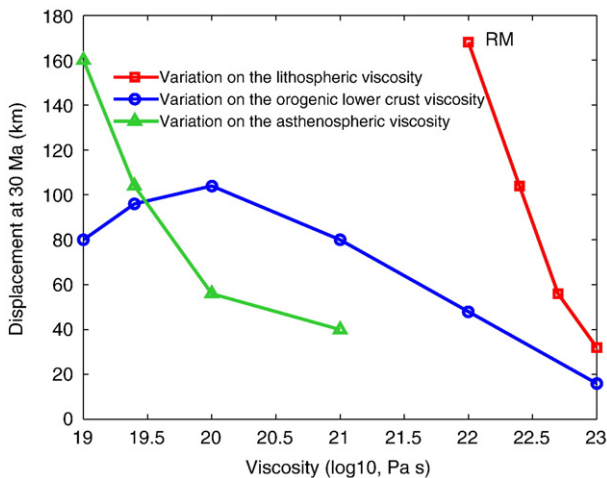


Fig. 3. Accumulated displacement of the delamination point after 30 Ma of evolution computed for different models varying the viscosity of the lithospheric mantle (μ_{max}), orogenic lower crust (μ_{LC}) and asthenosphere (μ_0).

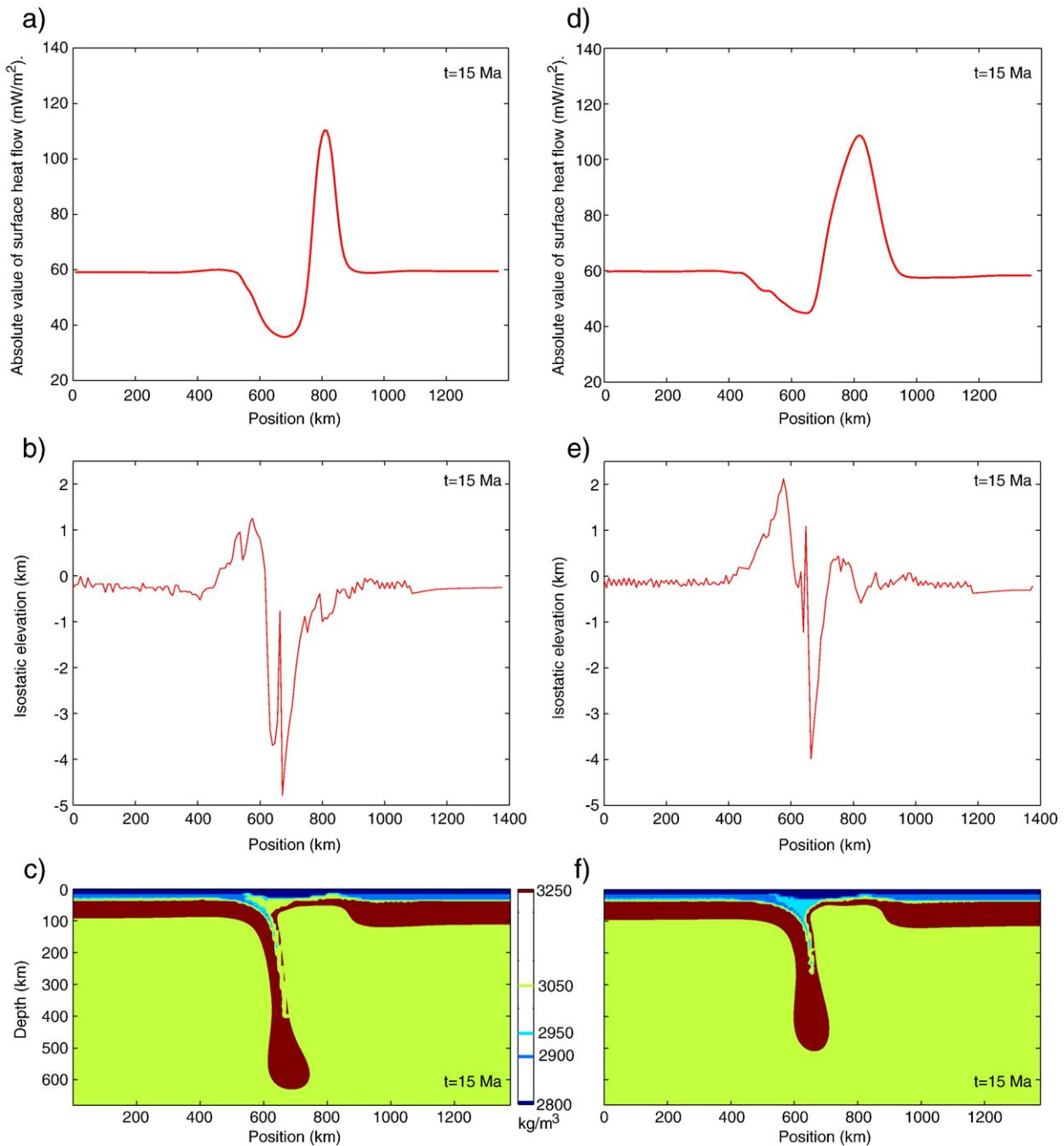


Fig. 5. Comparison after 15 Ma of evolution of the Reference Model with orogenic lower crust density of 3050 kg/m³ (a–c) and another model with a less dense lower crust of 2950 kg/m³ (d–f). The compared observables are the surface heat flow (a, d), the local isostatic topography (b, e) and the density distribution (c, f) showing only a series of discrete values for density.

counteracted by crustal thinning, thus resulting in a neutral topographic response. The maximum reached uplift is higher for the model with a less dense lower crust and the maximum subsidence is smaller, due to the shallower slab compared to the Reference Model. Short wavelength features (e.g. relative maximum elevation at about 620 km in the Reference Model) reflect strong lateral heterogeneities in the density distribution.

Fig. 6 shows predicted dynamic topography after 30 Ma of evolution of two models with exactly the same configuration and density as shown in Fig. 5, but introducing a ‘soft sediment’ upper layer. In these models, delamination develops more slowly than in models without this layer, because the isotherms distribution is

shifted upwards to include this new layer. Therefore the lithosphere is initially hotter and thermal negative buoyancy causing lithosphere sinking is reduced with respect to the models without a ‘soft sediment’ layer. In the model with a high density orogenic lower crust, the loading of the delaminating lithospheric mantle produces surface subsidence (to the left of about 600 km in Fig. 6a). Note that maximum subsidence is located just to the left of the delaminating slab, whereas the maximum subsidence predicted for isostatic elevation is located exactly above the slab. In contrast, this subsidence is not observed in the model with a lighter lower crust because the thickened and more buoyant crust overcomes the effect of slab sinking (which is, in turn, slower). In this second model,

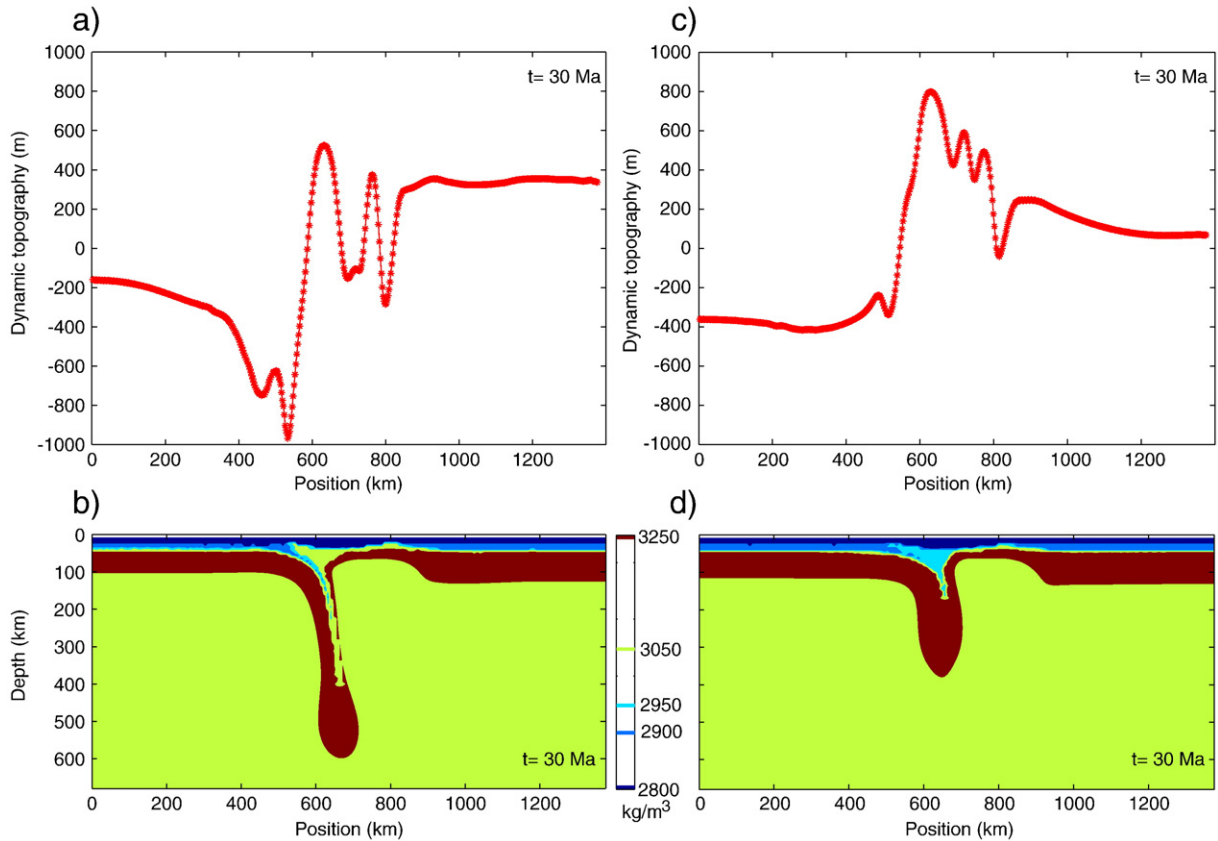


Fig. 6. Predicted dynamic topography (a, c) and density distribution (b, d) after 30 Ma of evolution of two models with 'soft sediments' upper layer. The model displayed at the left (a, b) has orogenic lower crust density of 3050 kg/m³ and the model displayed at the right (c, d) has orogenic lower crust density of 2950 kg/m³.

asthenospheric upwelling is shown to cause surface uplift over the area of thinned lithospheric mantle (Fig. 6c), but maximum uplift is nevertheless predicted over the region of maximum crustal thickening (at about 620 km in Fig. 6c). We therefore infer that the density of the lower crust has also a significant influence on the dynamic topography changes during delamination.

3.2. Models with lithospheric roots

Fig. 7 shows the evolution of a model with an initial setup consisting of a flat crust with a standard value of lower crust density (2950 kg/m³), and including a region of thickened lithospheric mantle. Delamination evolves faster in this model because the area occupied by the crustal root in previous models is now occupied by denser lithospheric mantle. This simulation highlights that, provided sufficient negative buoyancy to trigger lithospheric sinking, a thick low viscosity layer (represented by the lower crust) is not necessary to produce delamination. Moreover, we obtain the same pattern of crustal thickening/thinning associated to the migrating delamination point.

It is worth comparing our results with those by Göğüş and Pysklywec (2008b). These authors considered homogeneously thick lithospheric mantle (with an area of extra-density) and crust, and imposed a low viscosity zone in the lithospheric mantle including a horizontal channel along the base of the crust. The Moho position predicted by these authors, showing an anti-symmetric pattern, is rather different from that obtained here. They obtained that the downward deflection of the Moho has nearly the same amplitude and width as the area affected by upward Moho deflection. This discrepancy likely reflects a rather different model setup, as they did not make rheologic and/or density distinction between upper and

lower crust. Moreover, Göğüş and Pysklywec (2008b) considered non-Newtonian rheology everywhere except in the low viscosity zone, where they imposed a constant value for this viscosity.

Fig. 8 shows model-predicted surface heat flow, local isostatic topography and density distribution after 10 Ma of evolution. Compared to model with the same density but with orogenic crust (Fig. 5d), the heat flow is now higher (Fig. 8a) because the asthenosphere rises to shallower depths. Another difference is that the area of uplift obtained before, just to the left of the slab (Fig. 5e) does not appear now since the effect of the negatively buoyant slab overcomes that of positive buoyancy due to crustal thickening (Fig. 8b). The highly negative predicted topographic elevation is due to the strong mass excess in the lithospheric mantle imposed in this model. Similarly, the equivalent model including a layer of 'soft sediments' predicts surface subsidence for the same area above the delaminated lithospheric mantle (Fig. 9; note that a longer time of evolution, 23 Ma, is needed to reach a development of delamination similar to the model without this upper layer). Comparing the dynamic topography predicted with this initially flat crust model (Fig. 9a) with that predicted by the orogenic crust model (Fig. 6c) it can be inferred that the mass excess of the delaminating mantle lithosphere is high enough to switch from uplift to subsidence. Differently from Göğüş and Pysklywec (2008b), we do not obtain an area of surface uplift to the right of slab location. This discrepancy can be ascribed to the fact that these authors reproduce a much broader area of asthenospheric upwelling.

4. Concluding remarks

In this work we have numerically investigated the influence of the crustal structure and the density of the lower crust on the evolution of

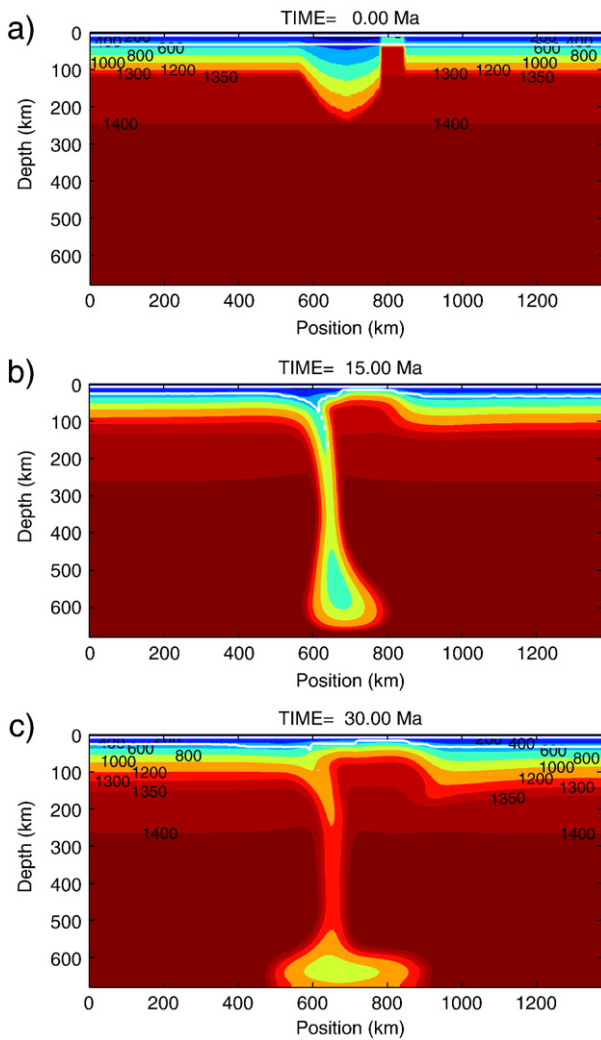


Fig. 7. Evolution of a model with an initial setup consisting of a flat crust with a standard value of lower crust density (2950 kg/m^3) and including a lithospheric root. Colors represent temperature distribution with labels in $^{\circ}\text{C}$; white lines show the bases of the upper and lower crust.

delamination considering different geodynamic scenarios suitable to develop this process. We have compared models with crustal and lithospheric roots (mimicking a post-collisional orogenic scenario) and models only with lithospheric roots (simulating a remnant slab). For both setups we obtain a migrating pattern of crustal thickening in front of the delamination point due to viscous drag, and crustal thinning behind the delamination point due to the asthenospheric upwelling. We therefore suggest that this pattern is a characteristic feature of the delamination mechanism, as it appears regardless of the initial crustal structure.

Our results show that a high density orogenic lower crust, likely related to the presence of eclogite, significantly accelerates the sinking of the delaminated mantle. The pattern of isostatic elevation is characterized by laterally migrating surface uplift/subsidence and is shown to be relatively insensitive to lower crust density variations. However, these density changes are better captured by the predicted dynamic topography. It shows surface subsidence adjacent to the delaminating lithospheric mantle for the model with a high density orogenic lower crust, and surface uplift above the slab for a model with a less dense orogenic lower crust. The uplift in this second model is explained by the effect of the positive buoyancy of the thickened

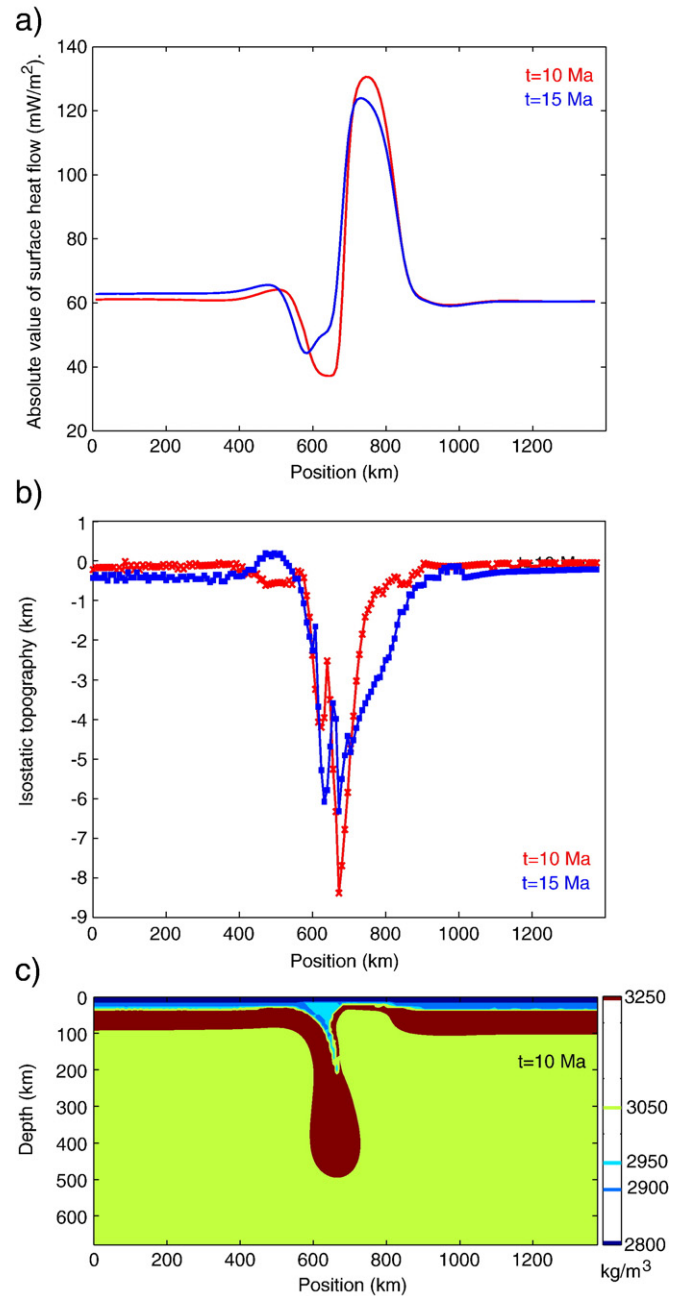


Fig. 8. Model-predicted surface heat flow (a), local isostatic topography (b) and density distribution (c) for model shown in Fig. 7 after 10 Ma of evolution.

crust that overcomes the effect of negative buoyancy of the delaminated lithospheric mantle.

Both isostatic and dynamic topographic responses of our models with initially flat crust are subsidence, due to the strong mass excess of the lithospheric root. This result highlights that, provided sufficient negative buoyancy, a thick low viscosity layer (represented by the lower crust) is not needed to produce delamination.

According to our modeling, there is not a specific characteristic pattern of topography changes associated with delamination, but results from the interplay between highly variable factors, as slab sinking velocity, asthenospheric upwelling and changes in crustal thickness. Therefore, caution must be taken when possible delamination processes are inferred only on the basis of topographic evolution.

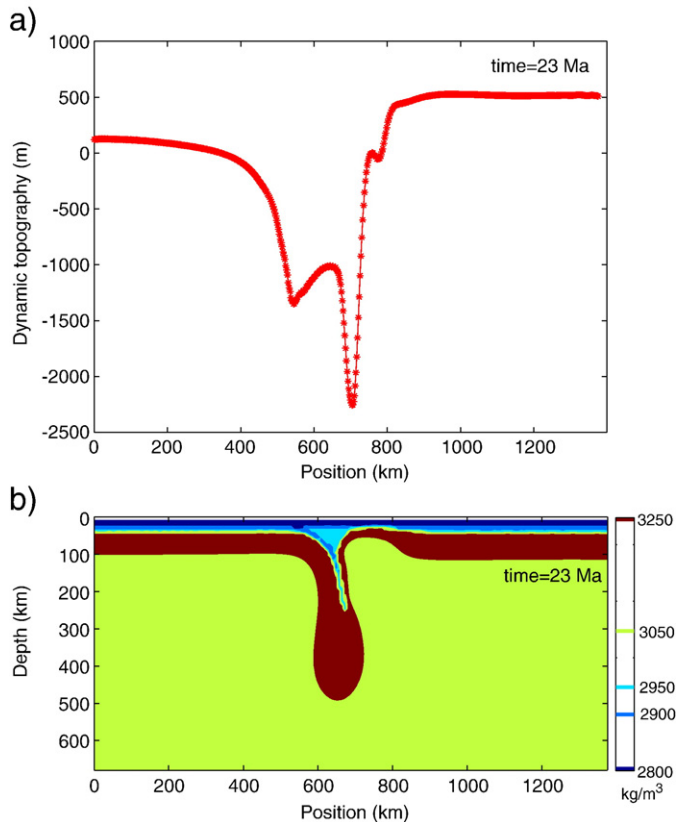


Fig. 9. Predicted dynamic topography (a) and density distribution (b) after 23 Ma of evolution for a model without crustal root but with lithospheric root and a 'soft sediments' upper layer. The model has orogenic lower crust density of 2950 kg/m^3 .

Acknowledgments

This work was funded by the Spanish Plan Nacional del MEC projects CTM2006-13666-C02-02/MAR and CGL2009-13103; and funding from UCM Research Groups. This is a contribution of the Consolider-Ingenio 2010 team CSD2006-00041 (TOPO-IBERIA). J. L. Valera acknowledges the support of a UCM grant. Calculations were partially carried out in the Fiswulf cluster of the Faculty of Physics.

References

- Anderson, J.D., 1995. *Computational Fluid Dynamics*. McGraw Hill, Inc.
- Arcay, E., Tric, E., Doin, M.-P., 2007. Slab surface temperature in subduction zones: influence of the interplate decoupling depth and upper plate thinning processes. *Earth Planet. Sci. Lett.* 255, 324–338.
- Arnold, J., Jacoby, W.R., Schmeling, H., Schott, B., 2001. Continental collision and the dynamic and thermal evolution of the Variscan orogenic crustal root – numerical models. *J. Geodyn.* 31, 273–291.
- Bird, P., 1978. Initiation of intracontinental subduction in the Himalaya. *J. Geophys. Res.* 83, 4975–4987.
- Bird, P., 1979. Continental delamination and the Colorado Plateau. *J. Geophys. Res.* 84, 7561–7571.
- Boussinesq, J., 1903. *Théorie analytique de la chaleur mise en harmonie avec la thermodynamique et avec la théorie de la lumière*, Volume II. Gauthier-Villars, Paris.
- Buck, W.R., Toksöz, M.N., 1983. Thermal effects of continental collisions: thickening a variable viscosity lithosphere. *Tectonophysics* 100, 53–69.
- Calvert, A., Sandvol, E., Seber, D., Barazangi, M., Roecker, S., Mourabit, T., Vidal, F., Alguacil, G., Jabour, N., 2000. Geodynamic evolution of the lithosphere and upper mantle beneath the Alboran Region of the Western Mediterranean: constraints from travel time tomography. *J. Geophys. Res.* 105, 10871–10898.
- Channel, J.E.T., Mareschal, J.C., 1989. Delamination and asymmetric lithospheric thickening in the development of the Thyrrenian Rift. In: Coward, M.P., Dietrich, D., Park, R.G. (Eds.), *Alpine Tectonics: Geol. Soc. Lond. Spec. Publ.*, 45, pp. 285–300.
- Conrad, C.P., Behn, M.D., Silver, P.G., 2007. Global mantle flow and the development of seismic anisotropy: differences between the oceanic and continental upper mantle. *J. Geophys. Res.* 112, B07317. doi:10.1029/2006JB004608.

- Ducea, M.N., Saleeby, J.B., 1998. A case for delamination of the deep batholithic crust beneath the Sierra Nevada, California. *Int. Geol. Rev.* 40 (1), 78–93.
- England, P.C., Houseman, G.A., 1989. Extension during continental convergence, with application to the Tibetan Plateau. *J. Geophys. Res.* 94, 17561–17579.
- Enns, A., Becker, T.W., Schmeling, H., 2005. The dynamics of subduction and trench migration for viscosity stratification. *Geophys. J. Int.* 120 (2), 761–775.
- Fleitout, L., Froidevaux, C., 1982. Tectonics and topography for a lithosphere containing density heterogeneities. *Tectonics* 1, 21–56.
- Gerya, T., Yuen, D.A., Maresch, W.V., 2004. Thermomechanical modelling of slab detachment. *Earth Planet. Sci. Lett.* 226, 101–116.
- Göğüş, O.H., Pysklywec, R.N., 2008a. Mantle lithosphere delamination driving plateau uplift and synconvergent extension in eastern Anatolia. *Geology* 36 (9), 723–726. doi:10.1130/G24982A.1.
- Göğüş, O.H., Pysklywec, R.N., 2008b. Near-surface diagnostics of dripping or delaminating lithosphere. *J. Geophys. Res.* 113, B11404. doi:10.1029/2007JB005123.
- Houseman, G., Molnar, P., 2001. Mechanisms of lithospheric rejuvenation associated with continental orogeny. In: Miller, J.A., Holdsworth, R.E., Buick, I.S., y Hand, M. (Eds.), *Continental Reactivation and Reworking: Geological Society, London, Special Publications*, 184, pp. 13–38.
- Houseman, G., Mackenzie, D., Molnar, P., 1981. Convective instability of a thickened boundary layer and its relevance for the thermal evolution of continental belts. *J. Geophys. Res.* 86 (B7), 6115–6132.
- Ita, J., King, S.D., 1994. Sensitivity of convection with an endothermic phase change to the form of governing equations, initial conditions, boundary conditions and equation of state. *J. Geophys. Res.* 99, 15919–15938.
- Jiménez-Munt, I., Fernández, M., Vergés, J., Platt, J.P., 2008. Lithosphere structure underneath the Tibetan plateau inferred from elevation, gravity and geoid anomalies. *Earth Planet. Sci. Lett.* 267, 276–289.
- Jull, M., Kelemen, P.B., 2001. On the conditions for lower crustal convective instability. *J. Geophys. Res.* 106 (B4), 6423–6446.
- Knapp, J.H., Knapp, C.C., Raileanu, V., Matenco, L., Mocanu, V., Dinu, C., 2005. Crustal constraints on the origin of mantle seismicity in the Vrancea Zone, Romania: the case for active continental lithospheric delamination. *Tectonophysics* 410, 311–323.
- Lachenbruch, A., Morgan, P., 1990. Continental extension, magmatism and elevation: formal relations and rules of thumb. *Tectonophysics* 174, 39–62.
- Le Pourhiet, L., Gurnis, M., Saleeby, J., 2006. Mantle instability beneath the Sierra Nevada Mountains in California and Death Valley extension. *Earth Planet. Sci. Lett.* 251, 104–119.
- Leech, M.L., 2001. Arrested orogenic development: eclogitization, delamination, and tectonic collapse. *Earth Planet. Sci. Lett.* 185, 149–159.
- Lenardic, A., Kaula, W.M., 1995. More thoughts on convergent crustal plateau formation and mantle dynamics with regard to Tibet. *J. Geophys. Res.* 100 (B8), 15,193–15,203.
- Lustrino, M., 2005. How the delamination and detachment of lower crust can influence basaltic magmatism. *Earth-Sci. Rev.* 72, 21–38.
- Manea, V., Gurnis, M., 2007. Subduction zone evolution and low viscosity wedges and channels. *Earth Planet. Sci. Lett.* 264, 22–45.
- Marotta, A.M., Fernández, M., Sabadini, R., 1998. Mantle unrooting in collisional settings. *Tectonophysics* 296, 31–46.
- Marotta, A.M., Fernández, M., Sabadini, R., 1999. The onset of extension during lithospheric shortening: a two-dimensional thermomechanical model for lithospheric unrooting. *Geophys. J. Int.* 139, 98–114.
- Marotta, A.M., Spelta, E., Rizzetto, C., 2006. Gravity signature of crustal subduction inferred from numerical modelling. *Geophys. J. Int.* 166, 923–938. doi:10.1111/j.1365-246X.2006.03058.x.
- Morency, C., Doin, M.P., 2004. Numerical simulations of the mantle lithosphere delamination. *J. Geophys. Res.* 109, B03410. doi:10.1029/2003JB002414.
- Negredo, A.M., Valera, J.L., Carminati, E., 2004. TEMSPOL: a MATLAB thermal model for deep subduction zones including major phase transformations. *Comput. Geosci.* 30, 249–258.
- Rüpke, L.H., Phipps-Morgan, J., Hort, M., Connolly, J.A.D., 2004. Serpentine and the subduction zone water cycle. *Earth Planet. Sci. Lett.* 223, 17–34.
- Schmeling, H., 1989. Compressible convection with constant and variable viscosity: the effect on slab formation, geoid and topography. *J. Geophys. Res.* 94 (B9), 12463–12481.
- Schmeling, H., Babeyko, A., Enns, A., Faccenna, C., Funicello, F., Gerya, T., Golabek, G., Grigull, S., Kaus, B., Morra, G., van Hunen, J., 2008. A benchmark comparison of spontaneous subduction models – towards a free surface. *Phys. Earth Planet. Inter.* 171, 198–223.
- Schott, B., Schmeling, H., 1998. Delamination and detachment of a lithospheric root. *Tectonophysics* 296, 225–247.
- Seber, D., Barazangi, M., Ibenbrahim, A., Demnati, A., 1996. Geophysical evidence for lithospheric delamination beneath the Alboran Sea and Rif-Betic mountains. *Nature* 379, 785–790.
- Tritton, D.J. (1988), *Physical Fluid Dynamics*, Oxford Clarendon Press, Oxford Science Publications, 519 p.
- Turcotte, L., 1983. Mechanisms of crustal deformation. *J. Geol. Soc. London* 140, 701–724.
- Valera, J.L., Negredo, A.M., Villaseñor, A., 2008. Asymmetric delamination and convective removal numerical modeling: comparison with evolutionary models for the Alboran Sea region. *Pure Appl. Geophys.* 165, 1683–1706. doi:10.1007/s00024-008-0395-8.
- Valera, J.L. (2009). *Development and application of numerical thermomechanical modeling of continental delamination processes*, Ph.D., Univ. Complutense de Madrid, 224 pp.
- Zandt, G., Gilbert, H., Owens, T.J., Ducea, M., Saleeby, J., Jones, C.H., 2004. Active foundering of a continental arc root beneath the southern Sierra Nevada in California. *Nature* 431, 41–46.